Optics Letters

Tailored optical potentials for Cs atoms above waveguides with focusing dielectric nano-antenna

Angeleene S. Ang,[1,2,4] Alexander S. Shalin,[3] and Alina Karabchevsky[1,2,*]

[1]School of Electrical and Computer Engineering, Ben-Gurion University of the Negev, Israel
[2]Center for Quantum Science and Technology (BGU-QST), Ben-Gurion University of the Negev, Israel
[3]ITMO University, 49 Kronversky Ave., St. Petersburg, Russia
[4]e-mail: angeleene.ang@gmail.com
*Corresponding author: alinak@bgu.ac.il

Received 14 April 2020; accepted 13 May 2020; posted 18 May 2020 (Doc. ID 394557); published 24 June 2020

Tuning the near field using all-dielectric nano-antennas offers a promising approach for trapping atoms, which could enable strong single-atom–photon coupling. Here we report the numerical study of an optical trapping of a single Cs atom above a waveguide with a silicon nano-antenna, which produces a trapping potential for atoms in a chip-scale configuration. Using counter-propagating incident fields, bichromatically detuned from the atomic cesium D-lines, we numerically investigate the dependence of the optical potential on the nano-antenna geometry. We tailor the near-field potential landscape by tuning the evanescent field of the waveguide using a toroidal nano-antenna, a configuration that enables trapping of ultracold Cs atoms. Our research opens up a plethora of trapping atoms applications in a chip-scale manner, from quantum computing to quantum sensing, among others.

https://doi.org/10.1364/OL.394557

Controlled positioning of atoms and molecules with extreme precision is a fascinating achievement in the field of quantum optics and photonics. Optical trapping was first shown by Ashkin in his seminal work (1970), where he trapped a dielectric microparticle (2018 Nobel Prize in Physics); in 1978, he suggested a three-dimensional trap for neutral atoms [1]. Since then, the optical trapping of particles and, specifically, atoms has been extensively investigated [2–4]. So far, the smallest optical atomic traps have been realized with dimensions of half an optical wavelength. However, this is not a fundamental limit. Atomic trapping can be achieved at even smaller distances—in the sub-wavelength regime—by tuning near fields in order to overcome the diffraction limit of far fields.

In the case of confining a particle much smaller than the wavelength of the trapping light (Rayleigh regime), the trapping force is directly proportional to the intensity gradient of the field. High-power lasers have conventionally been used to generate a strong intensity gradient, for the trapping and manipulation of particles. To address the need for high laser power, optical trapping using plasmonic nanostructures or metamaterials [5] has been proposed, because plasmonic systems allow for localization of an electromagnetic radiation at the nanoscale [6–11]. The plasmonic structures used in the aforementioned work are traditionally made of metals, which suffer from heating effects [12,13], leading to Johnson noise, and limited storage time of atom-based systems [14,15]. Previous works have, nevertheless, experimentally demonstrated atomic traps utilizing plasmonic structures [5,16–18]. On the other hand, photonic nanojets—narrow, high-intensity light beams emerging from the shadow side of dielectric micro/nanostructures—generated by spheres embedded on top of a substrate illuminated by a plane wave, have been proposed as possible optical atomic traps [19,20]. By removing the metallic element, an all-dielectric setup greatly reduces the noise. Such systems, e.g., based on optical fibers [21–24], can provide electric fields sufficient for trapping a atoms.

Here, we propose an all-dielectric system concept for which the silicon nano-antenna is placed on top of a dielectric waveguide as an alternative atomic trapping setup to mitigate the heating issues while trapping atoms. For this, we numerically investigate the dependence of the bichromatically constructed trapping potentials for cesium atoms on the shape of the nano-antenna. Figure 1 shows the schematics of the system we study: the counter-propagating incident bichromatic fields launched into both facets of the ridge waveguide to generate a standing wave for trapping along the propagation direction, and the silicon nano-antenna placed on the waveguide to localize the light further along the other directions.

To study the field focusing effect by different nano-antennas, we calculate optical potentials produced by hemispherical, cubic, conical, toroidal, and hemielliptical nano-antenna geometries, as shown in Fig. 2. We note that the field focused by the nano-antenna exhibits a global minimum of the optical potential, which corresponds to the presence of a stable atom trap. Unlike the conventional method of atom trapping with focused lasers, focusing with a nano-antenna can easily be integrated into a miniaturized setup. Unlike nanoplasmonic atomic

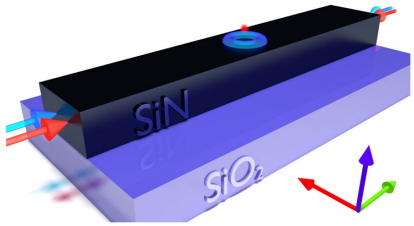

Fig. 1. Illustration of the studied all-optical atom trapping system with ridge waveguide, bi-chromatic incident light, the silicon nano-antenna atop, and with atom trapped (not to scale).

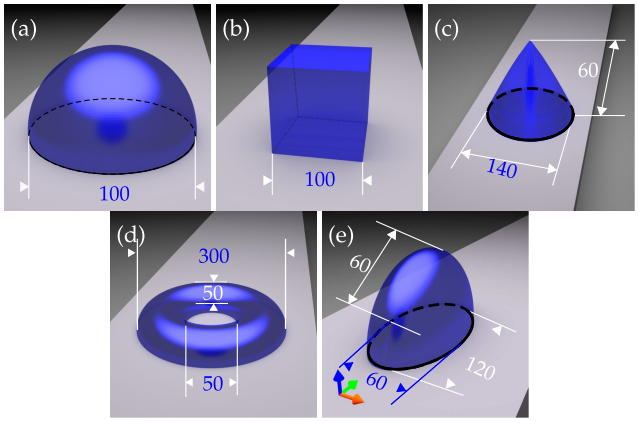

Fig. 2. Nano-antenna shapes and dimensions (all units in nm) considered for this paper (background not to scale).

lattices, the all-dielectric system proposed here is expected to reduce the harmful Johnson noise.

Fiber-based atom traps are created by illuminating a glass fiber from both end-facets to form a standing wave that, in turn, generates a trapping potential [21–24], but this type of atom trap is limited to trapping atoms along a line. The configuration studied here also utilizes a standing wave and, as we discuss below, also enables the possibility of scalable traps in two dimensions. The trapping fields used in the fiber-based systems use two laser wavelengths, one red-detuned with respect to the atomic optical transition ($\lambda_{\text{red}} = 1094$ nm) to create an attractive light force, and the other blue-detuned ($\lambda_{\text{blue}} = 652$ nm) to create a repulsive force. This is referred to as a bichromatic trapping system. The two fields together form an atom trap at the point where these forces are equal.

For linearly polarized incident light, each of these potentials is given by [2,25]

$$U_{\text{opt},j} = \frac{\pi c^2 \Gamma}{2\omega_0^3}\left(\frac{1}{\omega_j - \omega_1} + \frac{2}{\omega_j - \omega_2}\right) I_{\text{opt},j}, \qquad \textbf{(1)}$$

where $I_{\text{opt},j}$ and ω_j are, respectively, the light intensity at the surface and frequency corresponding to the two light fields (j designating "red" or "blue"), and $\Gamma = 2\pi \times 5.2$ MHz and ω_0, respectively, are the natural linewidth and average transition frequency of the excited atomic levels in the D line of cesium. The transition frequencies are ω_1 and ω_2, where the subscript refers to the sublevels D_1 ($6^2S_{1/2} \rightarrow 6^2P_{1/2}$ with transition wavelength of 852.3 nm) and D_2 ($6^2S_{1/2} \rightarrow 6^2P_{3/2}$ with transition wavelength 894.6 nm) [26]. Calculating the bichromatic optical potential on an ordinary featureless ridge waveguide yields a series of minima spaced by half the optical wavelength along the propagation direction, which is similar to results obtained from related work on atomic trapping using optical fibers [21–24].

A sharp optical intensity gradient is required to generate strong localized forces. To produce this intensity gradient, we introduce a perturbation in the boundary conditions, which, in this case, is the nano-antenna. We use silicon, a material with a high refractive index for visible–near infrared (VNIR) frequencies, in order to concentrate the energy from the waveguide at the near field of the nano-antenna. In our system, the evanescent field needs to be more pronounced along the z axis (i.e., towards the cladding where an atom is trapped), as opposed to the sides (i.e., along y); hence, we use the fundamental TM mode for the input field [27]. As shown in Eq. (1), the optical potential is directly proportional to the field intensity; hence, the optical potential can be written as [5,25]

$$U_j(z) = U_{0j}\exp(-2z/z_{0j}), \qquad \textbf{(2)}$$

where U_{0j} is the potential strength at the surface, and z_{0j} is the decay length of the evanescent wave. The potential dependence along x and y is calculated numerically. In order to take advantage of the evanescent wave's strong intensity gradient, the trap is designed such that the potential minimum is close to the surface.

We now consider an atomic trapping concept using a nano-antenna on a planar waveguide, as the geometry of the waveguide would naturally allow multiple (scalable) trapping potentials either along its length (as a line of atoms) or in two dimensions (as an array of atoms) by adding more nano-antennas. Placing nano-antennas on top of the waveguide does not affect the guided modes. This conclusion is supported by calculating the difference between the electric field magnitude with the nano-antenna ($|\mathbf{E}_{\text{na}}|$) and without ($|\mathbf{E}_{\text{wg}}|$), as shown in Fig. 3. This illustrates that the guiding layer is hardly perturbed by the presence of the nano-antenna; as can be seen, the maximum perturbation in the waveguide core, excluding the region near the nano-antenna, is less than 10%. It is well known that atomic lattices can be used as simulators to study strongly correlated quantum many-body systems [28]. By placing several nano-antennas in a 2D array, one can explore the atom–atom and atom–photon interactions in more than one dimension.

The silicon nitride (SiN) ridge waveguide on silica (SiO_2) substrate has dimensions of 1.56 μm along y and 0.534 μm along z to ensure 1) at least one confined quasi-TM mode; and 2) the evanescent tail of the fundamental TM mode allows for the sufficient penetration depth. Larger waveguides would excite the higher-order unnecessary modes' modal interference effects. The fields were calculated using Lumerical FDTD, with the fundamental TM mode launched into the waveguide.

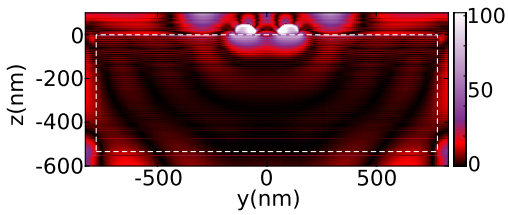

Fig. 3. Percent difference between the electric field magnitude in the waveguide without the nano-antenna ($|\mathbf{E}_{\text{wg}}|$) and with the nano-antenna ($|\mathbf{E}_{\text{na}}|$), calculated using $|(\mathbf{E}_{\text{na}} - \mathbf{E}_{\text{wg}})/\mathbf{E}_{\text{na}}|$. The dashed white rectangle indicates the boundaries of the guiding layer.

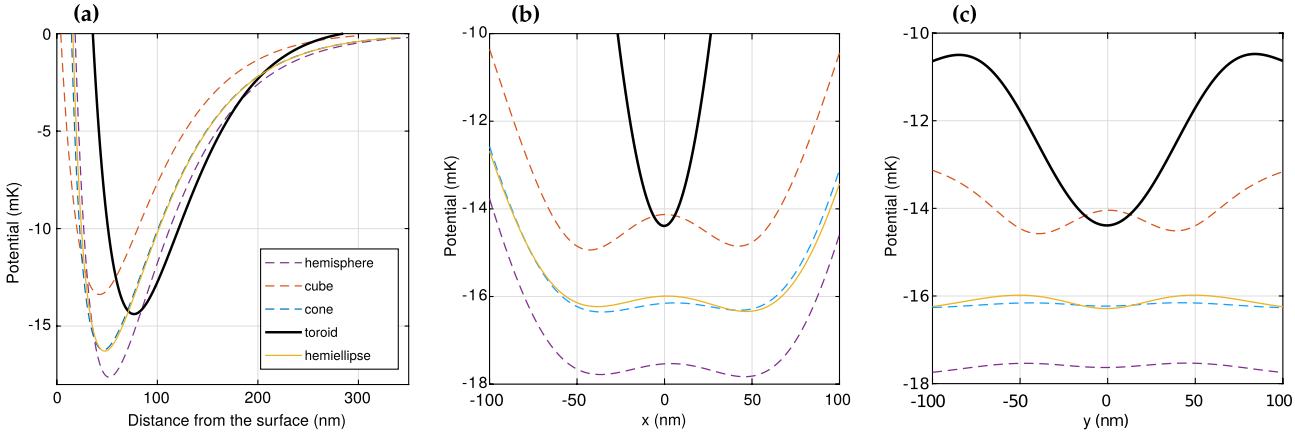

Fig. 4. Calculated (a) potential dependence on z, where $x = y = 0$; (b) potential dependence on x, where $z = z_d$ and $y = 0$; and (c) potential dependence on y, where $z = z_d$ and $x = 0$. While these potential curves are useful for characterizing the potential minimum, the global potential minimum is better presented as a three-dimensional isosurface at a given energy (see Fig. 5).

Sub-micrometer silicon nanostructures have been extensively studied in the field of all-dielectric resonators such as nanocubes, nanocones, and others [29]. Here we consider a cube and hemisphere for their simplicity in terms of fabrication [30]. In addition, to study nano-antenna characteristics that produce localized fields, we also consider a cone and a hemiellipse. A conical nano-antenna might provide better field localization in corners. The hemiellipse breaking symmetry might improve the field localization. To learn this, we show the total optical potential along Cartesian axes in Fig. 4 for those shapes. The sizes of the nano-antennas were selected to focus the fields on a subwavelength scale. We found that sizes smaller than about $\lambda/6$ do not localize the fields sufficiently.

More specific data from the simulations are shown in Table 1. We propose to illuminate the waveguide using the power scaling technique widely used in integrated photonics: rare-earth dopants can be used on a segment of the waveguide to amplify the source to achieve the listed fields [31]. We note that the effects of nonlinearity can be neglected because the contribution of the nonlinear coefficient [32] reads as Power $\times\ 2.88 * 10^{-7}$, and is negligible compared to the effective refractive index.

We consider two requirements before concluding that the potentials may be able to trap an atom. First, the optical trapping potential near its minimum must not be significantly perturbed by attractive atom-surface potentials that can destroy the trap near the surface. Second, the ground-state energy should lie within the potential well. We estimate the atom-surface potential U_{surf} using a MATLAB code that calculates approximate Casimir–Polder and van der Waals potentials using the equations described in Section III.B of Ref. [33], evaluated at $z = z_d$.

Table 1 compares U_{surf} to $U_{0,y}$ for each nano-antenna shape, where $U_{0,y}$ is the optical trapping potential along the y axis, i.e., the difference between the minimum and maximum of the curves shown in Fig. 4(c). Noting that the optical trapping force is dependent on the potential gradient, we see that this axis has the weakest trapping potential because of the shorter optical wavelength as compared to the width of the monomode waveguide. Table 1 also shows the ground-state energy $U_{\text{gs},z}$ calculated assuming a harmonic potential along the z axis (here we use the z axis because it has the highest frequency $\omega_z > \omega_x > \omega_y$ and therefore gives the greatest contribution to the approximate 3D ground-state energy $U_{\text{gs}} = \hbar(\omega_x + \omega_y + \omega_z)/2$).

Table 1. Calculated Numerical Results[a]

Structure	P_{red}	P_{blue}	z_d	$U_{0,y}$	$U_{\text{gs},z}$	U_{surf}
Hemisphere	6.1	16.9	52	0.25	0.86	0.2
Cube	6.1	16.2	43	0.53	1.07	0.4
Cone	6.1	17.8	42	0.21	0.86	0.5
Toroid	6.1	30.1	77	3.80	1.50	0.1
Hemiellipse	6.1	15.6	36	1.13	1.36	0.7

[a] P_{red} and P_{blue} are the respective powers (in watts) of the field source for the red- and blue-detuned sources, z_d is the distance (in nm) from the potential minimum to the nano-antenna surface, U_0 indicates the optical potential minimum (in mK), U_{gs} is the zero-point energy (in mK), and U_{surf} is the estimated atom-surface potential (in mK).

It is apparent from Table 1 that only the toroidal nano-antenna produces sufficiently strong potential along the y axis to support any bound states, i.e., the ground-state energy $U_{\text{gs},z}$ exceeds $U_{0,y}$ for all the other shapes, so they cannot support even a single bound state. The uniquely successful toroidal shape was chosen as one of the nano-antenna geometries considered in our study based on a previous paper [34] that reports a similar nano-antenna geometry generating an equilibrium force at the midpoint. We also note that the cross section of the field generated by the toroidal nano-antenna, is qualitatively similar to that shown in Ref. [34]. The toroidal nano-antenna also exhibits the lowest atom-surface potential U_{surf} for any of the shapes considered, partially because we have deliberately increased the blue-detuned laser power to push the potential minimum a little farther from the surface; as it is only a small fraction of the potential minimum at these distances, we do not consider U_{surf} further. In Fig. 5, we show an isopotential surface at the ground-state energy $U_{\text{gs},z}$ for the toroidal nano-antenna. This isopotential surface is completely closed, indicating at least qualitatively that an atom could indeed be trapped by the optical potential generated near such a nano-antenna. This more demanding test eliminates other geometries that we considered. We conclude that the dilectric nano-antenna of highly symmetric toroidal shape is the most suitable for atom trapping on a chip. Breaking the symmetry, in the case of the hemiellipse,

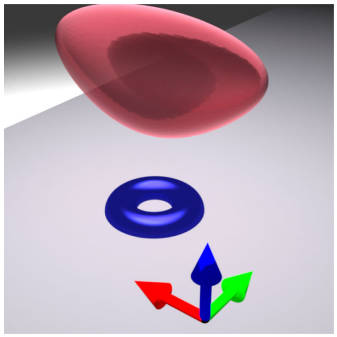

Fig. 5. Schematics of the potential isosurface at the zero-point energy for the toroidal nano-antenna.

improves the trap parameters, but not sufficiently for generating a closed isosurface at the zero-point energy.

For future perspective, bringing the atoms to distances below 100 nm from the nano-antenna surface may allow exploration of Casimir–Polder and van-der-Waals forces for the nano-antenna shapes considered here. This is a challenging theoretical problem as well as an experimental one, since the nano-antenna shape affects these forces qualitatively as well as quantitatively. Future work would also need to take into account the fabrication tolerances. It would also be interesting to explore heating effects that may be generated in such systems, as well as other possible mechanisms that can cause atoms to escape from the trap.

The temperature-associated effects such as in Ref. [35] are the subject of our future work. We would emphasize, however, that the potential trap generated on top of our all-dielectric system is essentially generated by the evanescent fields of the waveguide. For such a waveguide, the power carried by the evanescent field is about 0.08 of the overall power launched into the waveguide [27]; hence, the cladding region of the waveguide does not experience significant heating.

In conclusion, we have presented an optical trapping concept in an all-dielectric system, where a silicon nano-antenna produces a trapping potential for atoms in a chip-scale configuration. We numerically explored the dependence of the bichromatically constructed trapping potential on the nano-antenna shape. Our results show that the near-field-induced potential landscape can be tailored to sub-wavelength dimensions by manipulating the evanescent field using different nano-antenna geometries on top of the waveguide. We found that the dielectric toroidal nano-antenna generates an all-optical Cs atom trap directly above it. This trapping setup can be used as a method for trapping an array of single atoms with the advantage of the simplicity of integration within a silicon photonic platform, thereby paving the way toward fascinating atom–photon applications on a chip.

Funding. Israeli Innovation Authority Kamin Program (690); Russian Fund for Basic Research (18-02-00414, 18-72-1012, 20-52-00031).

Acknowledgment. A.S.S acknowledges the support of the Russian Fund for Basic Research within the projects 18-02-00414, 20-52-00031, 18-72-1012. A.S.A. thanks Mark Keil, Yonathan Japha, and David Groswasser for fruitful discussions.

Disclosures. The authors declare no conflicts of interest.

REFERENCES

1. A. Ashkin, Phys. Rev. Lett. **40**, 729 (1978).
2. R. Grimm, M. Weidemüller, and Y. B. Ovchinnikov, *Advances in Atomic, Molecular, and Optical Physics*, B. Bederson and H. Walther, eds. (Academic, 2000), Vol. **42**, pp. 95–170.
3. M. E. Kim, T.-H. Chang, B. M. Fields, C.-A. Chen, and C.-L. Hung, Nat. Commun. **10**, 1 (2019).
4. F. Nogrette, H. Labuhn, S. Ravets, D. Barredo, L. Béguin, A. Vernier, T. Lahaye, and A. Browaeys, Phys. Rev. X **4**, 021034 (2014).
5. C. Stehle, H. Bender, C. Zimmermann, D. Kern, M. Fleischer, and S. Slama, Nat. Photonics **5**, 494 (2011).
6. A. Karabchevsky, A. Mosayyebi, and A. V. Kavokin, Light Sci. Appl. **5**, e16164 (2016).
7. A. Karabchevsky, J. S. Wilkinson, and M. N. Zervas, Opt. Express **23**, 14407 (2015).
8. A. Karabchevsky, O. Krasnykov, M. Auslender, B. Hadad, A. Goldner, and I. Abdulhalim, Plasmonics **4**, 281 (2009).
9. A. Karabchevsky, S. Karabchevsky, and I. Abdulhalim, Sens. Actuators B **155**, 361 (2011).
10. A. Karabchevsky, I. Abdulhalim, C. Khare, and B. Rauschenbach, J. Nanophoton. **6**, 061508 (2012).
11. Y. Galutin, E. Falek, and A. Karabchevsky, Sci. Rep. **7**, 12076 (2017).
12. M. L. Brongersma and V. M. Shalaev, Science **328**, 440 (2010).
13. J. C. Ndukaife, V. M. Shalaev, and A. Boltasseva, Science **351**, 334 (2016).
14. M. E. Gehm, K. M. O'Hara, T. A. Savard, and J. E. Thomas, Phys. Rev. A **58**, 3914 (1998).
15. T. A. Savard, K. M. O'Hara, and J. E. Thomas, Phys. Rev. A **56**, R1095 (1997).
16. Z. Chen, F. Zhang, Q. Zhang, J. Ren, H. Hao, X. Duan, P. Zhang, T. Zhang, Y. Gu, and Q. Gong, Photon. Res. **5**, 436 (2017).
17. M. A. Zaman, P. Padhy, P. C. Hansen, and L. Hesselink, Appl. Phys. Lett. **112**, 091103 (2018).
18. Y. Tanaka, S. Kaneda, and K. Sasaki, Nano Lett. **13**, 2146 (2013).
19. V. Yannopapas, Opt. Commun. **285**, 2952 (2012).
20. V. Yannopapas and N. V. Vitanov, J. Phys. Condens. Matter **21**, 245901 (2009).
21. H. L. Sørensen, J.-B. Béguin, K. W. Kluge, I. Iakoupov, A. S. Sørensen, J. H. Müller, E. S. Polzik, and J. Appel, Phys. Rev. Lett. **117**, 133604 (2016).
22. N. V. Corzo, B. Gouraud, A. Chandra, A. Goban, A. S. Sheremet, D. V. Kupriyanov, and J. Laurat, Phys. Rev. Lett. **117**, 133603 (2016).
23. E. Vetsch, D. Reitz, G. Sagué, R. Schmidt, S. T. Dawkins, and A. Rauschenbeutel, Phys. Rev. Lett. **104**, 203603 (2010).
24. A. Goban, K. S. Choi, D. J. Alton, D. Ding, C. Lacroûte, M. Pototschnig, T. Thiele, N. P. Stern, and H. J. Kimble, Phys. Rev. Lett. **109**, 033603 (2012).
25. M. Mildner, A. Horrer, M. Fleischer, C. Zimmermann, and S. Slama, J. Phys. B **51**, 135005 (2018).
26. D. A. Steck, "Cesium D line data," (2003).
27. A. Katiyi and A. Karabchevsky, J. Lightwave Technol. **35**, 2902 (2017).
28. J. F. Sherson, C. Weitenberg, M. Endres, M. Cheneau, I. Bloch, and S. Kuhr, Nature **467**, 68 (2010).
29. P. D. Terekhov, K. V. Baryshnikova, Y. A. Artemyev, A. Karabchevsky, A. S. Shalin, and A. B. Evlyukhin, Phys. Rev. B **96**, 035443 (2017).
30. P. D. Terekhov, K. V. Baryshnikova, Y. Greenberg, Y. H. Fu, A. B. Evlyukhin, A. S. Shalin, and A. Karabchevsky, Sci. Rep. **9**, 1 (2019).
31. C. R. Smith, S. J. Beecher, J. I. Mackenzie, and W. A. Clarkson, Appl. Phys. B **123**, 225 (2017).
32. K. Ikeda, R. E. Saperstein, N. Alic, and Y. Fainman, Opt. Express **16**, 12987 (2008).
33. M. Rosenblit, Y. Japha, P. Horak, and R. Folman, Phys. Rev. A **73**, 063805 (2006).
34. Z. Xu and K. B. Crozier, Opt. Express **27**, 4034 (2019).
35. M. Spector, A. Ang, O. Minin, I. Minin, and A. Karabchevsky, "Temperature mediated 'photonic hook' nanoparticle manipulator with pulsed illumination," Nanoscale Adv., doi:10.1039/C9NA00759H .